

Discontinuities in Scalar Perturbations of Topological Black Holes

George Koutsoumbas,^{a,*} Eleftherios Papantonopoulos^{a,b}
and George Siopsis^{b,‡}

^aDepartment of Physics, National Technical University of Athens,
Zografou Campus GR 157 73, Athens, Greece

^bDepartment of Physics and Astronomy, The University of Tennessee, Knoxville, TN
37996 - 1200, USA

Abstract

We study the perturbative behaviour of topological black holes. We calculate both analytically and numerically the quasi-normal modes of scalar perturbations. In the case of small black holes we find discontinuities of the quasi-normal modes spectrum at the critical temperature and we argue that this is evidence of a second-order phase transition.

* kutsbas@central.ntua.gr

^b lpapa@central.ntua.gr

[‡] siopsis@tennessee.edu

1 Introduction

The knowledge of the spectrum of the quasi-normal modes (QNMs) is a powerful tool in the study of the late time behaviour of black holes. The QNMs are the complex frequencies by which a black hole responds if it is initially perturbed, and they do not depend on the details of the initial perturbation but rather on the intrinsic features of the black hole itself. The radiation associated with these modes is expected to be seen with gravitational wave detectors in the coming years, giving valuable information on the properties of black holes.

The QNMs of black holes in asymptotically flat spacetimes have been extensively studied and their spectrum was computed numerically and in many cases also analytically (for reviews, see [1, 2]). The advances in string theory and mainly the Anti-de Sitter - conformal field theory (AdS/CFT) correspondence has renewed the interest of computing the QNMs of black holes in asymptotically AdS spacetimes [3, 4, 5, 6, 7, 8]. Recent results from the Relativistic Heavy Ion Collider [9] show that a thermal quark-gluon plasma (QGP) is formed which is strongly coupled. The AdS/CFT correspondence provides the connection between the QGP and string black holes. In [10] the quasi-normal modes of AdS_5 -Schwarzschild black hole have been calculated and it was shown that they provide a dual description of the fluctuations of the QGP. Recently, in a more phenomenological approach, the AdS/CFT correspondence was applied to condensed matter physics [11]. It was shown [12] that fluctuations of the metric and the background electromagnetic field determines the conductivity of the boundary theory.

According to the AdS/CFT correspondence, a large static black hole in AdS corresponds to an (approximately) equilibrium thermal state in the CFT [14]. In ref. [4] it was shown that the QNMs for the scalar perturbations of large Schwarzschild-AdS black holes scaled with the temperature and it was argued that the perturbed system in the dual description will approach to thermal equilibrium of the boundary conformal field theory. However, when the black hole size is comparable to the AdS length scale there is a clear departure from this behaviour. It was then conjectured that this behaviour may be connected with a Hawking-Page phase transition [15, 16] which occurs when the temperature lowers.

For small black holes the behaviour of QNMs is not very well understood. For the case of Schwarzschild-AdS black holes the QNMs do not scale linearly with the temperature any more and their connection with the boundary conformal field theory is not clear. In [17, 18] we studied the QNMs of electromagnetic and gravitational perturbations of topological black holes (TBHs) in AdS spacetime coupled to a scalar or an electromagnetic field. For small black holes, compared to the length scale of the AdS space, we found that the QNMs behave quite differently from the QNMs of large black holes. Near the critical temperature purely dissipative modes appeared in the spectrum and the QNMs change slope around that point. We attributed this behaviour to a second order phase transition of the charged TBH towards the AdS vacuum solution.

In the literature there is a discussion of possible connections between the classical and thermodynamical properties of black holes [19]. In particular the question whether the knowledge of the QNM spectrum can give information about thermodynamical phase transitions in a wider class of black holes has recently gained considerable interest. It was suggested in [20] that the Dirac and Rarita-Schwinger perturbations are related to ther-

modynamic phase transitions of charged black holes. This has been criticised in [21], the argument being that the relation between the QNMs and the phase transition had not been properly formulated. In this direction, the discontinuities observed in the heat capacity of charged Kaluza-Klein black holes with squashed horizons, were connected with the quasi-normal spectrum [22]. Further evidence of a non-trivial relation between the thermodynamical and dynamical properties of black holes was provided in [23].

In this work we calculate both analytically and numerically the QNMs of scalar perturbations of topological-AdS black holes in $d = 4, 5$ and 6 dimensions. In all dimensionalities considered, we find a discontinuity of the QNMs spectrum at the critical point. This provides further evidence of a second order phase transition at the critical point observed in [17, 18]. In our numerical calculations we used the method developed in [4]. We conjecture that this method is problematic for large n because it breaks down, and a regularization scheme is proposed.

Our work is organized as follows: in section 2 the analytical calculation is presented, section 3 contains comments on the numerical method used, and in section 4 the numerical results may be found. Finally the conclusions are presented in section 5.

2 Analytical Calculation

Analytical results for the QNMs of topological black holes are only known for the massless case. In four dimensions they were calculated in [30] while a generalization to d -dimensions have been presented in [31]. For the general case early numerical results have been discussed in [3] and in [29]. To study the phase transition in topological black holes the QNM spectrum has to be known, at least near the critical point. Therefore in this section we calculate analytically the QNMs of scalar perturbations of topological black holes in various dimensions. At the critical point the mass goes to zero so we reproduce the known exact results. Also we discuss the asymptotic form of QNMs for large black holes. In five dimensions we present analytical results expressible through the Heun function. The analytical results will give us a clear indication of a second order phase transition around the critical point which will be substantiated by numerical results presented in the next section.

We consider the bulk action

$$I = \frac{1}{16\pi G} \int d^d x \sqrt{-g} \left[R + \frac{(d-1)(d-2)}{l^2} \right], \quad (2.1)$$

in asymptotically AdS_d where G is the Newton's constant and l is the AdS radius. The presence of a negative cosmological constant ($\Lambda = -\frac{(d-1)(d-2)}{2l^2}$) allows the existence of black holes with a topology $\mathbb{R} \times \Sigma$, where Σ is a $(d-2)$ -dimensional manifold of constant negative curvature. These black holes are known as topological black holes. The simplest solution of this kind reads

$$ds^2 = -f(r)dt^2 + \frac{dr^2}{f(r)} + r^2 d\sigma^2, \quad f(r) = r^2 - 1 - \frac{2\mu}{r^{d-3}}, \quad (2.2)$$

where we employed units in which the AdS radius is $l = 1$ and $d\sigma$ is the line element of Σ . The latter is locally isomorphic to the hyperbolic manifold H^{d-2} and of the form

$$\Sigma = H^{d-2}/\Gamma \quad , \quad \Gamma \subset O(d-2, 1) \quad , \quad (2.3)$$

where Γ is a freely acting discrete subgroup (i.e., without fixed points) of isometries. The geometry of the topological black holes as well their basic properties have been studied extensively in the literature [24]-[33].

The configurations (2.2) are asymptotically locally AdS spacetimes. It has been shown in [34] that the massless configurations where Σ has negative constant curvature are stable under gravitational perturbations. More recently the stability of the TBHs was discussed in [35].

We shall calculate analytically the quasi-normal modes of scalar perturbations of these black holes following the method discussed in [18]. A numerical approach will be discussed in section 3.

Massless scalar perturbations obey the radial wave equation

$$\frac{1}{r^{d-2}}(r^{d-2}f(r)\Phi')' + \frac{\omega^2}{f(r)}\Phi - \frac{\xi^2 + (\frac{d-3}{2})^2}{r^2}\Phi = 0 \quad . \quad (2.4)$$

By defining

$$\Phi = r^{-\frac{d-2}{2}}\Psi \quad (2.5)$$

the wave equation can be cast into a Schrödinger-like form,

$$-\frac{d^2\Psi}{dr_*^2} + V[r(r_*)]\Psi = \phi^2\Psi \quad , \quad (2.6)$$

in terms of the tortoise coordinate defined by

$$\frac{dr_*}{dr} = \frac{1}{f(r)} \quad , \quad (2.7)$$

and the potential is given by

$$V(r) = f(r) \left\{ \frac{d(d-2)}{4} + \frac{k^2 - \frac{3}{4}}{r^2} + \frac{(d-2)^2\mu}{2r^{d-1}} \right\} \quad , \quad k^2 = \xi^2 + \left(\frac{d-3}{2}\right)^2 \quad . \quad (2.8)$$

For later convenience we define $\Lambda = k^2 - 3/4$.

To obtain analytic expressions for the quasi-normal frequencies, it is convenient to introduce the coordinate

$$u = \left(\frac{r_+}{r}\right)^2 \quad . \quad (2.9)$$

The wave equation (2.6) becomes

$$4u^{3/2}\hat{f}(u)(u^{3/2}\hat{f}(u)\Psi')' + [\hat{\omega}^2 - \hat{V}]\Psi = 0 \quad , \quad \hat{\omega} = \frac{\omega}{r_+} \quad , \quad (2.10)$$

where prime denotes differentiation with respect to u and we have defined

$$\begin{aligned}\hat{f}(u) &\equiv \frac{f(r)}{r_+^2} = \frac{1}{u} - \frac{1}{r_+^2} - \frac{2\mu}{r_+^{d-1}} u^{\frac{d-3}{2}}, \\ \hat{V}(u) &\equiv \frac{V(r)}{r_+^2} = \hat{f}(u) \left\{ \frac{d(d-2)}{4} + \hat{\Lambda}u + \frac{(d-2)^2\mu}{2r_+^{d-1}} u^{\frac{d-1}{2}} \right\},\end{aligned}\quad (2.11)$$

and

$$\hat{\Lambda} = \frac{\Lambda}{r_+^2}, \quad 2\mu = r_+^{d-3}(r_+^2 - 1). \quad (2.12)$$

2.1 Exact solution in $d = 5$

In five dimensions ($d = 5$) we may solve the wave equation in terms of a Heun function and use the latter to determine the spectrum exactly albeit numerically. By factoring $\hat{f}(u)$,

$$\hat{f}(u) = (1-u) \left(\frac{1}{u} + 1 - \frac{1}{r_+^2} \right)$$

we may obtain an exact solution to the wave equation in terms of a Heun function,

$$\Psi(u) = u^{-3/4} \left(u + \frac{1}{1 - 1/r_+^2} \right)^{-\frac{\hat{\omega}\sqrt{1-1/r_+^2}}{2(2-1/r_+^2)}} (1-u)^{-\frac{i\hat{\omega}}{2(2-1/r_+^2)}} \text{Heun}(a, q, \alpha, \beta, \gamma, \delta, 1-u) \quad (2.13)$$

The Heun function obeys the equation

$$z(z-1)(z-a)F'' - [(-\alpha-\beta-1)z^2 + ((\delta+\gamma)a - \delta + \alpha + \beta + 1)z - a\gamma]F' - [-\alpha\beta z + q]F = 0 \quad (2.14)$$

and the various constants are

$$\begin{aligned}a &= \frac{2 - \frac{1}{r_+^2}}{1 - \frac{1}{r_+^2}}, \quad q = \frac{1}{2(1 - \frac{1}{r_+^2})(2 - \frac{1}{r_+^2})^2} \left[\frac{1}{2r_+^2}(\xi^2 + 1)(2 - \frac{1}{r_+^2})^2 + i\hat{\omega}(2 - \frac{1}{r_+^2}) \right. \\ &\quad \left. - \hat{\omega}^2(2 - \frac{3}{2r_+^2}) + \hat{\omega}(i\hat{\omega} - 2 + \frac{1}{r_+^2})(1 - \frac{1}{r_+^2})^{3/2} \right], \\ \alpha &= \beta = -\frac{(i + \sqrt{1 - \frac{1}{r_+^2}})\hat{\omega}}{2(2 - \frac{1}{r_+^2})}, \quad \gamma = 1 - \frac{i\hat{\omega}}{2 - \frac{1}{r_+^2}}, \quad \delta = -1.\end{aligned}$$

It behaves nicely at the horizon ($u \rightarrow 1$). Requiring $\Psi(0) = 0$ yields the constraint

$$\text{Heun}(a, q, \alpha, \beta, \gamma, \delta, 1) = 0, \quad (2.15)$$

which may be solved for $\hat{\omega}$ to obtain the quasi-normal frequencies of scalar modes in five dimensions.

2.2 Large Black Holes

For large black holes, we let $\hat{\omega}, \hat{\Lambda} \rightarrow 0$, $r_+ \rightarrow \infty$. The wave equation becomes

$$u^{3/2}[(u^{1/2} - u^{d/2})\Psi']' - \frac{(d-2)[d + (d-2)u^{\frac{d-1}{2}}]}{16}\Psi = 0 . \quad (2.16)$$

Two linearly independent solutions are

$$\Psi = u^{-\frac{d-2}{4}} , \quad u^{-\frac{d-2}{4}} \ln \left(1 - u^{\frac{d-1}{2}} \right) . \quad (2.17)$$

Both are unacceptable as they diverge at $u = 0, 1$, respectively. It follows that the only possible frequencies are those which diverge as $r_+ \rightarrow \infty$.

In five dimensions, the lowest mode may be deduced from the exact constraint in the limit $r_+ \rightarrow \infty$ keeping ξ and $\hat{\omega}$ fixed (and therefore $\hat{\Lambda} \rightarrow 0$, $\omega \sim r_+$). In this limit,

$$a = 2 , \quad q = \frac{[2(i-1) + (i-2)\hat{\omega}]\hat{\omega}}{8} , \quad \alpha = \beta = -\frac{(i+1)\hat{\omega}}{4} , \quad \gamma = 1 - \frac{i\hat{\omega}}{2} , \quad \delta = -1 .$$

The lowest frequency in five dimensions is found to be

$$\hat{\omega} = 3.12 - 2.75i \quad (2.18)$$

in agreement with earlier numerical results [4]. Therefore, for a large black hole, $\omega \sim r_+$ and QNMs do not contribute to the macroscopic (hydrodynamic) behaviour of the gauge theory fluid on the AdS boundary.

2.3 Near the Critical Point

At the critical point ($r_+ = 1$, $\mu = 0$), the wave equation reduces to

$$4u^{1/2}(u^{1/2}(1-u)\Psi')' + \left[\frac{\omega^2}{1-u} - \frac{d(d-2)}{4u} - \Lambda \right] \Psi = 0 . \quad (2.19)$$

The solution which is well-behaved at the boundary is

$$\Psi(u) = (1-u)^{-i\omega/2} u^{d/4} F\left(\frac{\frac{d+1}{2} + i\xi - i\omega}{2}, \frac{\frac{d+1}{2} - i\xi - i\omega}{2}; \frac{d+1}{2}; u\right) . \quad (2.20)$$

At the horizon, $u \rightarrow 1$, it behaves as

$$\Psi(u) \sim \mathcal{A}_+(1-u)^{-i\omega/2} + \mathcal{A}_-(1-u)^{i\omega/2} , \quad \mathcal{A}_{\pm} = \frac{\Gamma(\frac{d+1}{2})\Gamma(\pm i\omega)}{\Gamma(\frac{\frac{d+1}{2} - i\xi \pm i\omega}{2})\Gamma(\frac{\frac{d+1}{2} + i\xi \pm i\omega}{2})} . \quad (2.21)$$

Demanding $\mathcal{A}_- = 0$, we deduce the quasi-normal frequencies

$$\omega_n = \pm \xi - i \left(2n + \frac{d+1}{2} \right) , \quad n = 0, 1, 2, \dots \quad (2.22)$$

which have finite real part (except in the special case $\xi = 0$). This result agrees with the quasi-normal frequencies of massless topological black holes which they were calculated analytically for the first time in [30].

The hypergeometric functions corresponding to the eigenfunctions are polynomials. Explicitly,

$$\begin{aligned}\Psi_0(u) &= A_0(1-u)^{-i\xi/2-(d+1)/4}u^{d/4}, \\ \Psi_1(u) &= A_1(1-u)^{-i\xi/2-(d+5)/4}u^{d/4} \left[1 + \frac{2(1+i\xi)}{d+1}u \right],\end{aligned}\quad (2.23)$$

etc. They are orthogonal under the inner product (no complex conjugation!)

$$\langle n|m \rangle \equiv \int_0^1 \frac{du}{u^{1/2}(1-u)} \Psi_n(u) \Psi_m(u) \quad (2.24)$$

defined by appropriate analytic continuation of the parameter ξ . To normalize them ($\langle n|n \rangle = 1$), choose

$$A_0^2 = \frac{\Gamma(-i\xi)}{\Gamma(-i\xi - \frac{d+1}{2})\Gamma(\frac{d+1}{2})}, \quad A_1^2 = \frac{(d+1)\Gamma(-1-i\xi)}{(-2i\xi - d - 3)\Gamma(-i\xi - \frac{d+5}{2})\Gamma(\frac{d+1}{2})}, \quad (2.25)$$

etc.

Moving away from the critical point, the frequencies shift by

$$\delta\omega_n = \frac{1}{2\omega_n} \frac{\langle n|\mathcal{H}'|n \rangle}{\langle n|n \rangle}, \quad (2.26)$$

where

$$\mathcal{H}'\Psi_n = r_+^2 \left[-4u^{3/2}\hat{f}(u) \left(u^{3/2}\hat{f}(u)\Psi_n' \right)' + \hat{V}(u)\Psi_n \right] - \omega_n^2\Psi_n, \quad (2.27)$$

and we applied standard first-order perturbation theory.

We obtain

$$\begin{aligned}\delta\omega_0 &= -i(r_+ - 1) \frac{2^d\Gamma(\frac{d}{2})\Gamma(-i\xi)}{\sqrt{\pi}\Gamma(-i\xi + \frac{d-3}{2})}, \\ \delta\omega_1 &= -i(r_+ - 1) \frac{2^{d-2}\Gamma(\frac{d}{2})\Gamma(-i\xi - 1)[-2i\xi(d+1) - d^2 + 6d - 17]}{\sqrt{\pi}\Gamma(-i\xi + \frac{d-3}{2})}.\end{aligned}\quad (2.28)$$

For small ξ , there is no change in the imaginary part at first order. Below the critical point ($r_+ < 1$), the change in the real part is negative ($\delta\omega_n < 0$) and the real part decreases. There are critical values of ξ (determined by $\xi + \delta\omega_n \approx 0$),

$$\xi_0 \approx \sqrt{\frac{2^d\Gamma(\frac{d}{2})}{\sqrt{\pi}\Gamma(\frac{d-3}{2})}}\sqrt{1-r_+}, \quad \xi_1 \approx \sqrt{\frac{2^{d-2}\Gamma(\frac{d}{2})[d^2 - 6d + 17]}{\sqrt{\pi}\Gamma(\frac{d-3}{2})}}\sqrt{1-r_+} \quad (2.29)$$

below which the corresponding mode does not propagate (purely dissipative mode). It turns out that for $\xi < \xi_n$ pairs of purely dissipative modes emerge.

Above the critical point ($r_+ > 1$), $\delta\omega_n > 0$ and the real parts of the modes increase. The modes do not become purely dissipative for any value of ξ .

Also notice that below the critical point, $\delta\omega_n$ increases with n , therefore the real part decreases with n (positive slope) whereas above the critical point we obtain a *negative* slope for propagating modes.

These results will be discussed further along with a comparison with numerical results in section 4.

3 Numerical Calculation

In this section we present the numerical calculation of the QNMs of scalar perturbations of small topological black holes following the method developed by Horowitz and Hubeny [4].

After performing the transformation $\Psi(r) = \frac{\psi_\omega(r)}{r^{\frac{d-2}{2}}} e^{-i\omega r_*}$, the wave equation becomes

$$f(r) \frac{d^2 \psi_\omega(r)}{dr^2} + \left(\frac{df(r)}{dr} - 2i\omega \right) \frac{d\psi_\omega(r)}{dr} = V(r) \psi_\omega(r) . \quad (3.1)$$

The change of variables $r = 1/x$ yields an equation of the form

$$s(x) \left[(x - x_+)^2 \frac{d^2 \psi_\omega(x)}{dx^2} \right] + t(x) \left[(x - x_+) \frac{d\psi_\omega(x)}{dx} \right] + u(x) \psi_\omega(x) = 0 ,$$

where $x_+ = 1/r_+$ and $s(x)$, $t(x)$ and $u(x)$ are given by

$$\begin{aligned} s(x) &= \sum_k s_k (x - x_+)^k , \\ t(x) &= \sum_k t_k (x - x_+)^k , \\ u(x) &= \sum_k u_k (x - x_+)^k . \end{aligned}$$

Expanding the wave function around the (inverse) horizon x_+ ,

$$\psi_\omega(x) = \sum_0^\infty a_n(\omega) (x - x_+)^n , \quad (3.2)$$

we arrive at a recurrence formula for the coefficients,

$$a_n(\omega) = -\frac{1}{P_{n,0}} \sum_{m=n-4}^{n-1} P_{m,n-m} a_m(\omega) , \quad (3.3)$$

$$P_{m,n-m} \equiv m(m-1)s_{n-m} + mt_{n-m} + u_{n-m} . \quad (3.4)$$

We note that the few coefficients $a_m(\omega)$ with negative index m which will appear for $n < 2$ should be set to zero, while $a_0(\omega)$ is set to one. Since the wave function should vanish at infinity ($r \rightarrow \infty, x = 0$), we deduce

$$\psi_\omega(0) \equiv \sum_0^\infty a_n(\omega)(-x_+)^n = 0 . \quad (3.5)$$

The solutions of this equation are precisely the quasi-normal frequencies.

The change of variables

$$\bar{a}_n \equiv a_n x_+^n \quad , \quad \bar{P}_{m,n-m} \equiv P_{m,n-m} x_+^{n-m} = m(m-1)\bar{s}_{n-m} + m\bar{t}_{n-m} + \bar{u}_{n-m} \quad (3.6)$$

transforms eqs. (3.3) and (3.5) into

$$\bar{a}_n = -\frac{1}{\bar{P}_{n,0}} \sum_{m=n-4}^{n-1} \bar{P}_{m,n-m} \bar{a}_m , \quad (3.7)$$

and

$$\psi_\omega(0) \equiv \sum_0^\infty \bar{a}_n(\omega)(-1)^n = 0 , \quad (3.8)$$

respectively.

To get a feeling about the solutions of the recurrence relations we consider the limit of very large n . In this limit we may keep just the terms of order n^2 , so relation (3.6) is approximated by

$$\bar{P}_{m,n-m} \simeq m^2 \bar{s}_{n-m} \quad (3.9)$$

and the recurrence relation reads

$$\bar{a}_n = -\frac{1}{\bar{s}_0} \sum_{m=n-N}^{n-1} \bar{s}_{n-m} \bar{a}_m .$$

Notice that it has constant coefficients, so it can be solved analytically. For simplicity let us restrict attention to the case $N = 4$. The solution of the recurrence relation reads

$$\bar{a}_n = \frac{K_1}{r_1^n} + \frac{K_2}{r_2^n} + \frac{K_3}{r_3^n} + \frac{K_4}{r_4^n} .$$

It should be emphasized that the coefficients K_m ($m = 1, 2, 3, 4$) do not depend on n . Explicitly,

$$K_m = \frac{\mathcal{A}_m}{\mathcal{B}_m} ,$$

where

$$\begin{aligned} \mathcal{A}_m &\equiv \bar{s}_0 * (\bar{A}_3 * r_m^3 + \bar{A}_2 * r_m^2 + \bar{A}_1 * r_m + \bar{A}_0) + \bar{s}_1 * (\bar{A}_2 * r_m^3 + \bar{A}_1 * r_m^2 + \bar{A}_0 * r_m) \\ &\quad + \bar{s}_2 * (\bar{A}_1 * r_m^3 + \bar{A}_0 * r_m^2) + \bar{s}_3 * (\bar{A}_0 * r_m^3) , \\ \mathcal{B}_m &\equiv -(4 * \bar{s}_4 * r_m^4 + 3 * \bar{s}_3 * r_m^3 + 2 * \bar{s}_2 * r_m^2 + \bar{s}_1) . \end{aligned}$$

r_m are the four roots of the equation

$$\bar{s}_0 + \bar{s}_1 r_m + \bar{s}_2 r_m^2 + \bar{s}_3 r_m^3 + \bar{s}_4 r_m^4 = 0 , \quad (3.10)$$

respectively and \bar{A}_k , $k = 0, 1, 2, 3$ are the values of the first four coefficients which are necessary to completely specify the solution.

For large n , the sum is dominated by the root which has the smallest absolute value. If all roots have an absolute value which is bigger than one, the coefficients will go to zero for large n and the method is expected to work. However, if the absolute value of one of the roots is smaller than one, we run into problems. In our case, one of the roots is equal to -1 .

To see this, we report expressions for various coefficients in table 1. Using these, one

i	\bar{s}_i	\bar{t}_i	\bar{u}_i
0	$x_+(x_+^2 - 3)$	$-3x_+ + x_+^3 + 2i\omega x_+^2$	0
1	$x_+(4x_+^2 - 9)$	$-12x_+ + 6x_+^3 + 4i\omega x_+^2$	$-3x_+ + (\frac{3}{4} - \xi^2)x_+^3$
2	$x_+(6x_+^2 - 10)$	$-18x_+ + 12x_+^3 + 2i\omega x_+^2$	$-3x_+ + (\frac{3}{2} - 2\xi^2)x_+^3$
3	$x_+(4x_+^2 - 5)$	$-12x_+ + 10x_+^3$	$-3x_+ + (\frac{11}{4} - \xi^2)x_+^3$
4	$x_+(x_+^2 - 1)$	$-3x_+ + 3x_+^3$	$-x_+ + x_+^3$

Table 1: Coefficients used in the numerical method (eq. (3.6))

may show that

$$\bar{P}_{n,0} + \bar{P}_{n-2,2} + \bar{P}_{n-4,4} = \bar{P}_{n-1,1} + \bar{P}_{n-3,3} .$$

Notice that this equality holds exactly in $d = 4$. For $d = 5, 6$ the two sums differ by an amount which is of order $\mathcal{O}(1)$ so it is negligible for large n . In particular one may show the relation

$$\bar{s}_0 + \bar{s}_2 + \bar{s}_4 = \bar{s}_1 + \bar{s}_3 ,$$

which implies that -1 is a root of eq. (3.10), as advertised.

Thus our case is inconclusive and one should examine $\frac{1}{n}$ corrections to settle the issue of convergence. We expect that $|\frac{\bar{a}_{n+1}}{\bar{a}_n}| = 1 + \frac{\mu}{n}$. If $\mu < 0$ the sequence will converge to zero and the series can be finite. Otherwise there is a problem with convergence.

To ensure convergence and obtain numerical solutions of the equations $\Re[\psi_\omega(0)] = 0$, $\Im[\psi_\omega(0)] = 0$, we shall introduce a regularization scheme as follows: rather than imposing the condition that the wave function vanish at $r = \infty$, we impose the condition that it vanish at $r = R = \frac{r_\pm}{\epsilon}$, $\epsilon \ll 1$. This translates to $x = X = \epsilon x_+$. Then eq. (3.5) is replaced by

$$\psi_\omega(X) \equiv \sum_0^\infty a_n(\omega)(X - x_+)^n = 0 \Rightarrow \sum_0^\infty \bar{a}_n(\omega)(-1)^n(1 - \epsilon)^n = 0 . \quad (3.11)$$

Asymptotically, $\bar{a}_n(\omega) = (-1)^n A(\omega)$ which solves the recursion relation and is confirmed by numerical results. Without the regularization parameter ($\epsilon = 0$), this leads to problems

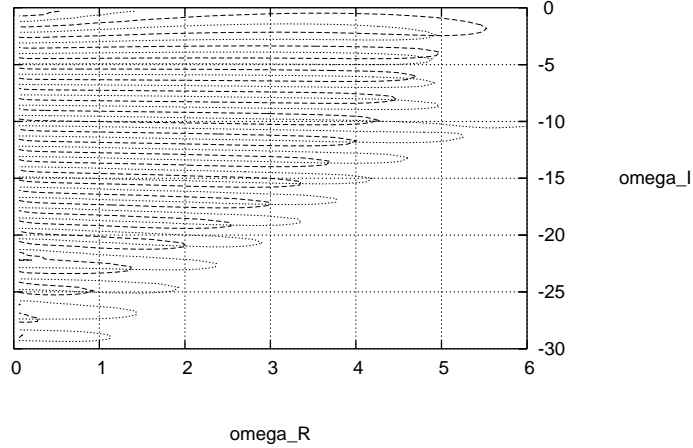


Figure 1: Scalar QNMs in four dimensions at $r_+ = 0.95, \xi = 5.0$.

because the left-hand side of (3.8) diverges. With a finite ϵ , the series is asymptotically geometric and converges.

If ϵ is small enough, the error introduced is negligible. However, choosing too small a value for ϵ is not computationally efficient as it may call for too many terms in the series (so that the individual terms become small enough). We have used $\epsilon = 0.01$ for $d = 4, d = 5$, and $\epsilon = 0.02$ for $d = 6$. With these values our results agree with the analytical results for $r_+ \approx 1$.

4 Results

4.1 $d = 4$

We start with the case $r_+ = 0.95$ (below the critical point), $\xi = 5.0$, depicted in figure 1. We observe that there exists a finite number of QNMs and positive slope. Similar results may be seen in figure 2, corresponding to $r_+ = 0.99$ and $\xi = 5.0$. In the latter case the real parts do not change as much between successive modes. Going to smaller values of ξ the most important changes are that the region of propagating modes becomes smaller, while the real parts take smaller values. This is apparent upon inspection of figure 3 (for $\xi = 3.0$) and figure 4 (for $\xi = 1.0$). In the latter case purely dissipative modes appear. There exist no modes at all for imaginary parts absolutely larger than 35.. The purely dissipative modes disappear for larger values of ξ ; for $\xi = 2$ it is difficult to detect them. This fact is consistent with the analytic result that there exist critical values of ξ , above which only propagating modes exist. Thus, for small enough values of ξ we have several propagating modes with relatively small absolute values of their imaginary parts and positive slope,

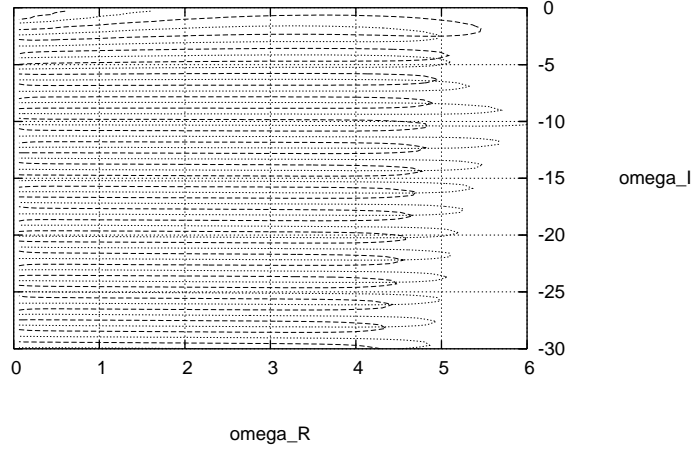


Figure 2: Scalar QNMs in four dimensions at $r_+ = 0.99, \xi = 5.0$.

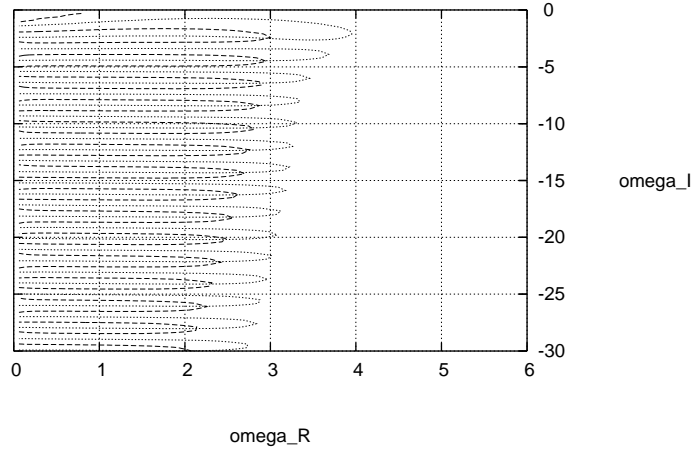


Figure 3: Scalar QNMs in four dimensions at $r_+ = 0.99, \xi = 3.0$.

followed by a finite number of purely dissipative modes. For larger values of ξ only a finite number of propagating modes exists.

To illustrate the features of the case with $r_+ > 1.0$, (above the critical point), we give in figure 5 the results for $r_+ = 1.10$, $\xi = 1.0$. The slope is negative right from the beginning

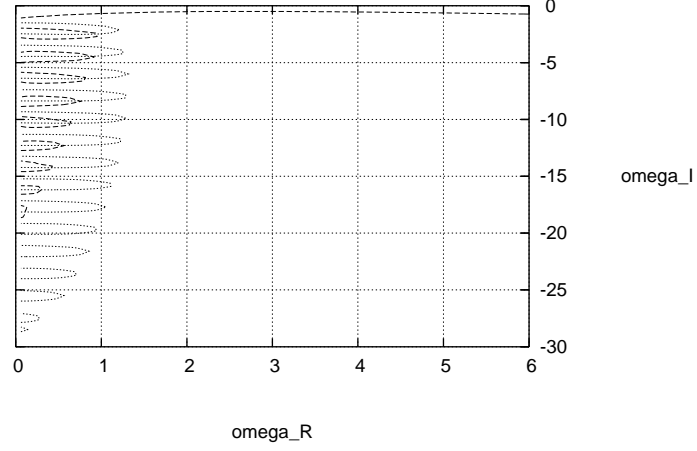


Figure 4: Scalar QNMs in four dimensions at $r_+ = 0.99, \xi = 1.0$.

and no purely dissipative modes emerge.

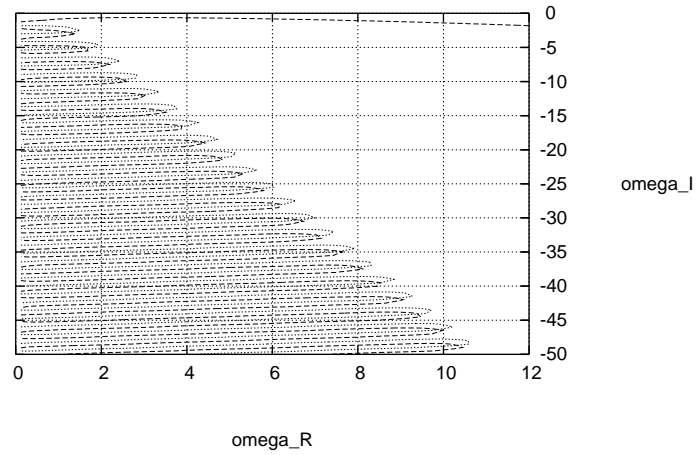


Figure 5: Scalar QNMs in four dimensions at $r_+ = 1.10, \xi = 1.0$

Another set of results refers to the lowest modes, in particular the behaviour of their real parts as functions of ξ . The analytical results derived from eq. (2.28) along with the

numerical results are shown in figure 6. The agreement is good and it improves for large values of ξ . In particular, values of ξ where these two real parts vanish compare quite well with the analytically computed values.

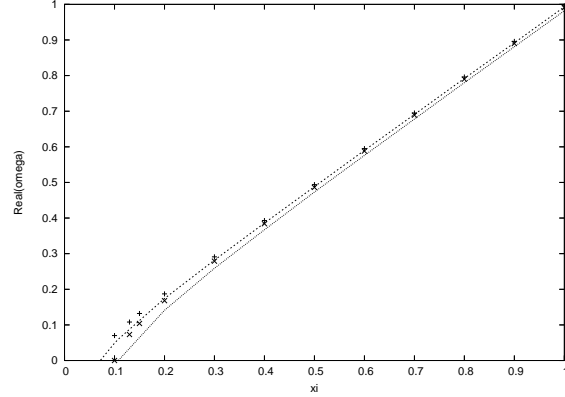


Figure 6: The analytical results (eq. (2.28)) for the real parts of the two lowest QNMs ω_0 and ω_1 vs ξ for $d = 4$ and $r_+ = 0.999$ are represented by lines, while their numerical counterparts by points. The upper (lower) curve and the corresponding points represent ω_0 (ω_1).

In figure 7 we show the dependence of the critical values ξ_0 and ξ_1 on the horizon r_+ . This figure depicts the analytical results expressed by eq. (2.29), as well as the corresponding numerical results. The agreement between the two approaches is quite good.

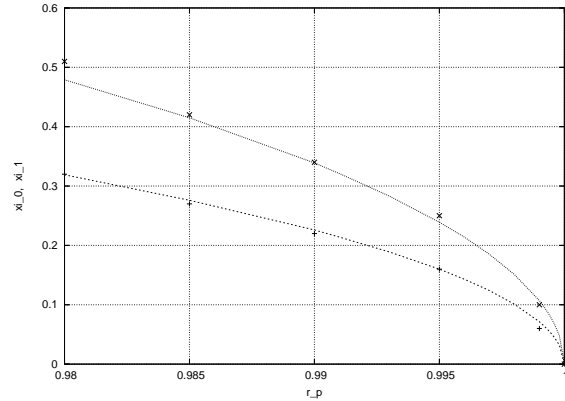


Figure 7: The points represent numerical estimates of the critical values ξ_0 and ξ_1 as functions of the horizon for $d = 4$, while lines give the corresponding analytical estimates (eq. (2.29)). The larger (lower) values represent ξ_0 (ξ_1).

Agreement between analytical (eqs. (2.22) and (2.28)) and numerical results for the two lowest QNMs is further demonstrated in table 2. Let us comment that the two biggest critical values for ξ in this case occur for $r_+ = 0.95$ and read $\xi_0 = 0.50$, $\xi_1 = 0.76$, well below the values of ξ considered here. The agreement is better as we approach the value $r_+ = 1.0$, as is evident in the last four rows of table 2.

ξ	r_+	ω_0^{anal}	ω_0^{num}	ω_1^{anal}	ω_1^{num}
1.0	0.95	$0.64 - 2.23i$	$0.80 - 2.36i$	$0.11 - 3.89i$	$0.42 - 4.17i$
3.0	0.95	$2.80 - 2.32i$	$2.90 - 2.42i$	$2.51 - 4.08i$	$2.75 - 4.30i$
5.0	0.95	$4.85 - 2.36i$	$4.93 - 2.44i$	$4.63 - 4.16i$	$4.81 - 4.34i$
1.0	0.99	$0.93 - 2.44i$	$0.96 - 2.47i$	$0.82 - 4.38i$	$0.91 - 4.44i$
5.0	0.99	$4.97 - 2.47i$	$4.99 - 2.49i$	$4.93 - 4.43i$	$4.96 - 4.47i$
5.0	0.999	$4.9971 - 2.4972i$	$4.9985 - 2.4986i$	$4.9926 - 4.4932i$	$4.9963 - 4.4965i$
5.0	0.9995	$4.9985 - 2.4986i$	$4.9993 - 2.4993i$	$4.9963 - 4.4966i$	$4.9981 - 4.4982i$
5.0	0.9999	$4.9997 - 2.4997i$	$4.9998 - 2.4998i$	$4.9993 - 4.4993i$	$4.9996 - 4.4996i$

Table 2: Comparison of analytic *vs* numerical results for the two lowest QNMs at $d = 4$

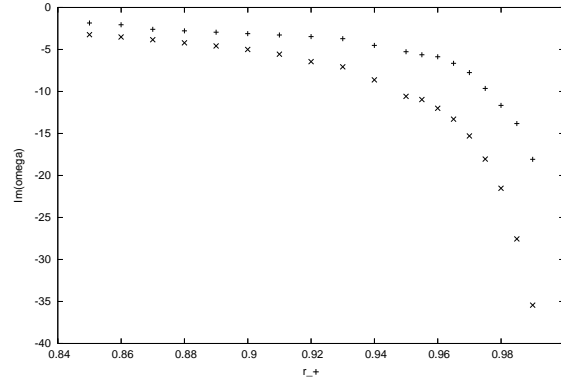


Figure 8: Imaginary part of the lowest purely dissipative QNM in four dimensions *vs* r_+ for $\xi = 1.0$ (crosses) and $\xi = 2.0$.

Finally we depict in figure 8 the behaviour of the lowest purely dissipative QNM as a function of r_+ for $\xi = 1.0$ and $\xi = 2.0$. It tends to $-\infty$ as the horizon approaches the critical value $r_+ = 1$.

4.2 $d = 5$ and $d = 6$

Only quantitative changes appear in the five-dimensional case. We depict sample results in figure 9. Comparing against figure 3, let us only note the quantities $|\Re(\omega)|$ change more between successive modes. We also note that in five dimensions the propagating modes coexist with purely dissipative modes in the same range of imaginary parts. Of course, there are no propagating modes with sufficiently large values of $|\Im(\omega)|$, i.e., the propagating modes disappear and only dissipative modes survive.

As one moves to $d = 6$, numerical difficulties become more severe and QNMs with too large imaginary parts become increasingly harder to explore. We show sample results in figure 10. It seems that we encounter a qualitative change. The propagating QNMs have positive slope in the region of (absolutely) small imaginary parts, then there is a number of purely dissipative modes, while for even larger imaginary parts a new branch appears,

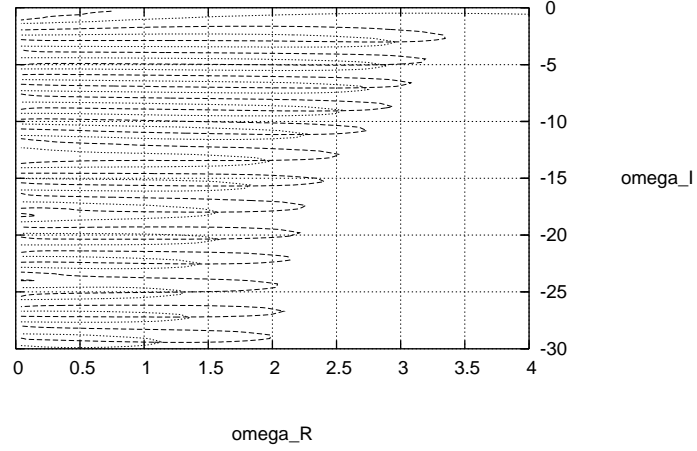


Figure 9: Scalar QNMs in five dimensions at $r_+ = 0.99, \xi = 3.0$

which has negative slope.

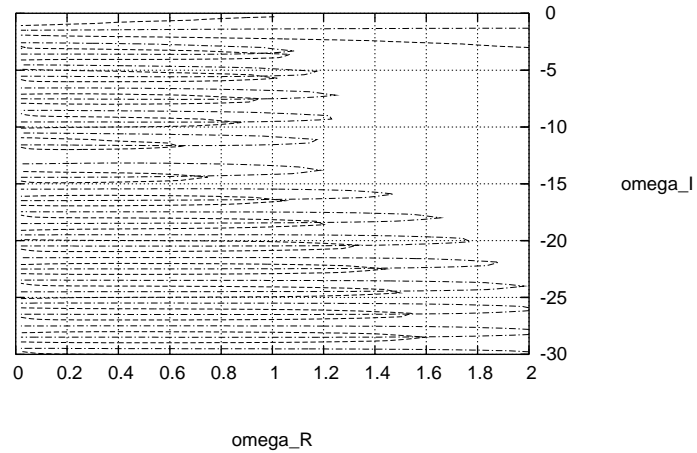


Figure 10: Scalar QNMs in six dimensions at $r_+ = 0.9999, \xi = 1.0$.

We also study the real parts of the lowest modes for $d = 5$ as functions of ξ and present both the analytical results derived from eq. (2.28) and their numerical counterparts in

figure 11. The numerical results lie a bit above the prediction and the agreement is not so good as in the $d = 4$ case. This feature is even more pronounced for $d = 6$. The results are depicted in figure 12. It is evident that the most sizeable discrepancies occur for ω_1 . In particular, the numerical results appear more steep and the corresponding critical value for ξ_1 is substantially bigger than the analytical prediction. These results show that first-order perturbation theory is inadequate in this case - one needs to include higher-order perturbative effects.

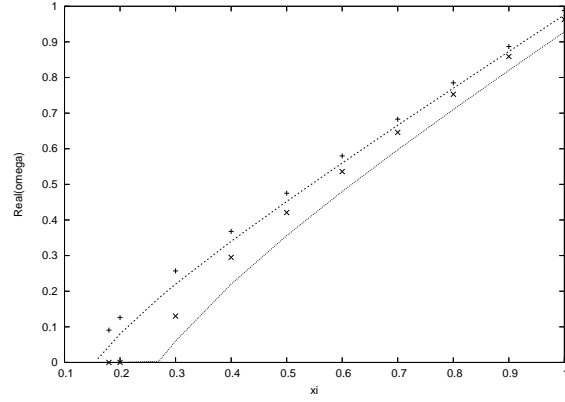


Figure 11: The analytical results (eq. (2.28)) for the real parts of the two lowest QNMs ω_0 and ω_1 vs ξ for $d = 5$ and $r_+ = 0.999$ are represented by lines, while their numerical counterparts by points. The upper (lower) curve and the corresponding points represent ω_0 (ω_1).

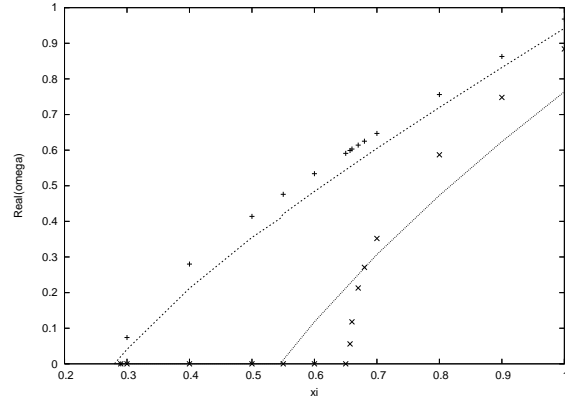


Figure 12: The analytical results (eq. (2.28)) for the real parts of the two lowest QNMs ω_0 and ω_1 vs ξ for $d = 6$ and $r_+ = 0.999$ are represented by lines, while their numerical counterparts by points. The upper (lower) curve and the corresponding points represent ω_0 (ω_1).

In figure 13 we show the dependence of the critical values ξ_0 and ξ_1 on the horizon r_+ in five dimensions. This figure depicts both the analytical results expressed by equation (2.29) and the corresponding numerical results. Similar results are presented in figure 14

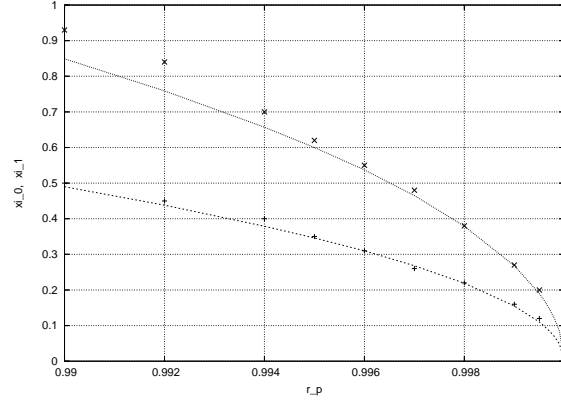


Figure 13: The points represent numerical estimates of the critical values ξ_0 and ξ_1 as functions of the horizon for $d = 5$, while lines give the corresponding analytical estimates (eq. (2.29)). The larger (lower) values represent ξ_0 (ξ_1).

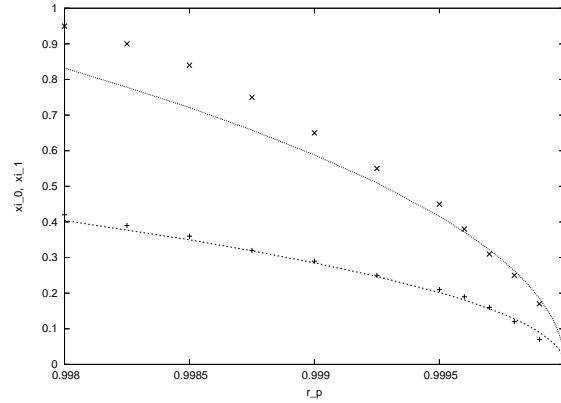


Figure 14: The points represent numerical estimates of the critical values ξ_0 and ξ_1 as functions of the horizon for $d = 6$, while lines give the corresponding analytical estimates (eq. (2.29)). The larger (lower) values represent ξ_0 (ξ_1).

for six dimensions. The agreement between analytical and numerical results is satisfactory in all cases.

Table 3 contains the comparison of analytical versus numerical results for the two lowest QNMs at $d = 5$. The agreement is fairly good. Let us comment that the two critical values for ξ read in this case: $\xi_0 = 1.09$, $\xi_1 = 1.90$ for $r_+ = 0.95$ and and smaller for the remaining values of r_+ . The values of ξ considered lie above the critical values.

Table 4 contains the comparison of analytic versus numerical results for the two lowest QNMs at $d = 6$. The agreement is fairly good. Let us comment that the two critical values for ξ read: $\xi_0 = 0.90$, $\xi_1 = 1.86$ for $r_+ = 0.99$. They are smaller for the remaining values of r_+ . The values of ξ considered lie above the critical values.

In figure 15 we show exact values of the imaginary part of the lowest purely dissipative mode for $\xi = 1$ and $\xi = 2$ versus r_+ for $d = 5$, along with a fit encoding the divergence at the critical point $r_+ = 1$. These results are successfully reproduced numerically as can easily be seen in figure 16. The corresponding results for $d = 6$, where no analytical results

ξ	r_+	ω_0^{anal}	ω_0^{num}	ω_1^{anal}	ω_1^{num}
3.0	0.95	$2.60 - 3.00i$	$2.82 - 3.02i$	$1.80 - 5.00i$	$2.43 - 5.17i$
5.0	0.95	$4.76 - 3.00i$	$4.89 - 3.01i$	$4.28 - 5.00i$	$4.67 - 5.05i$
3.0	0.99	$2.92 - 3.00i$	$2.96 - 3.00i$	$2.76 - 5.00i$	$2.88 - 5.00i$
5.0	0.99	$4.95 - 3.00i$	$4.97 - 3.00i$	$4.86 - 5.00i$	$4.93 - 5.00i$
5.0	0.999	$4.9952 - 3.0000i$	$4.9976 - 3.0000i$	$4.9856 - 5.0000i$	$4.9928 - 5.0000i$
5.0	0.9995	$4.9976 - 3.0000i$	$4.9988 - 3.0000i$	$4.9928 - 5.0000i$	$4.9964 - 5.0000i$
5.0	0.9999	$4.9995 - 3.0000i$	$4.9998 - 3.0000i$	$4.9986 - 5.0000i$	$4.9993 - 5.0000i$

Table 3: Comparison of analytic *vs* numerical results for the two lowest QNMs at $d = 5$

ξ	r_+	ω_0^{anal}	ω_0^{num}	ω_1^{anal}	ω_1^{num}
3.0	0.99	$2.89 - 3.58i$	$2.91 - 3.65i$	$2.59 - 5.78i$	$3.06 - 5.77i$
5.0	0.99	$4.95 - 3.54i$	$4.81 - 3.61i$	$4.82 - 5.64i$	$4.90 - 5.97i$
5.0	0.999	$4.9951 - 3.5042i$	$4.9822 - 3.5140i$	$4.9822 - 5.5141i$	$5.0027 - 5.5393i$
5.0	0.9995	$4.9976 - 3.5021i$	$4.9911 - 3.5071i$	$4.9911 - 5.5070i$	$5.0015 - 5.5193i$
5.0	0.9999	$4.9995 - 3.5004i$	$4.9982 - 3.5014i$	$4.9982 - 5.5014i$	$5.0003 - 5.5038i$

Table 4: Comparison of analytic *vs* numerical results for the two lowest QNMs at $d = 6$

are available, are contained in figure 17.

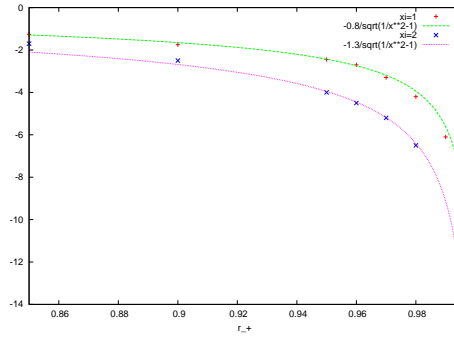


Figure 15: Exact results for the imaginary part of the lowest purely dissipative mode for $\xi = 1$ and $\xi = 2$ *vs* r_+ for $d = 5$.

5 Conclusions

We have studied the perturbative behaviour of the topological-AdS black holes. We have calculated both analytically and numerically the QNMs of scalar perturbations of these black holes.

Analytical calculations show that for small black holes at any dimension there is a critical point (at $r_+ = 1$) below which the real part decreases with n , having a positive

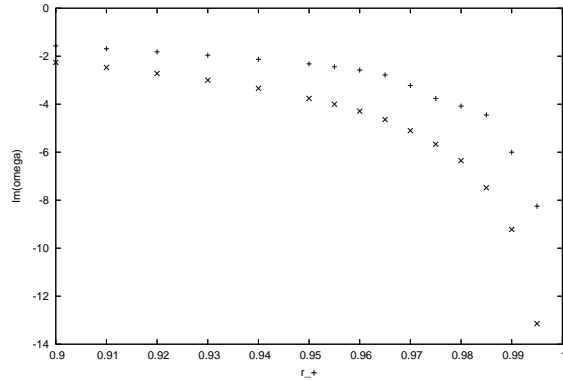


Figure 16: Numerical results for the results for the imaginary part of the lowest purely dissipative QNM in five dimensions *vs* r_+ for $\xi = 1.0$ (crosses) and $\xi = 2.0$.

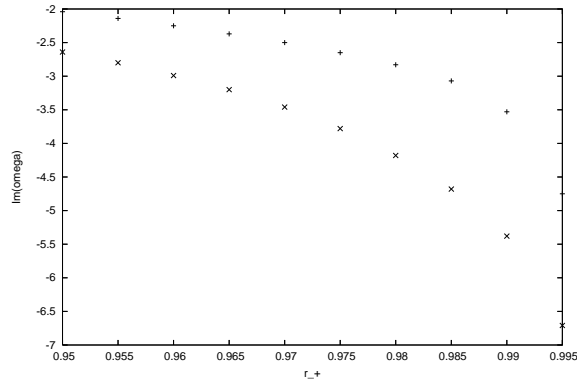


Figure 17: Imaginary part of the lowest purely dissipative QNM in six dimensions *vs* r_+ for $\xi = 1.0$ (crosses) and $\xi = 2.0$.

slope, whereas above the critical point the oscillatory modes increase with a negative slope. We also found that below the critical point there is a critical value of ξ below which there are purely decaying modes while above the critical point there are only oscillatory modes for any ξ . In five dimensions the QNMs of scalar perturbations of TBH-AdS can be obtained explicitly from the Heun function which solves the five-dimensional wave equation.

These results are also supported by numerical investigations of the QNMs. The numerical results show clearly a change of slope of QNMs around a critical temperature for dimensions $d = 4, 5, 6$. For larger dimensions the root finding algorithm is difficult to be implemented. This is connected with the observation that for higher dimensional theories the regularization needed for the convergence of the series becomes less efficient.

Acknowledgments

We thank E. Berti and V. Cardoso for their comments. Work supported by the NTUA research program PEVE07. G. S. was supported in part by the US Department of Energy under grant DE-FG05-91ER40627.

References

- [1] K. D. Kokkotas and B. G. Schmidt, Living Rev. Rel. **2**, 2 (1999) [arXiv:gr-qc/9909058].
- [2] H.-P. Nollert, Class. Quant. Grav. **16** (1999) R159.
- [3] J. S. F. Chan and R. B. Mann, Phys. Rev. D **55**, 7546 (1997) [arXiv:gr-qc/9612026]; Phys. Rev. D **59**, 064025 (1999).
- [4] G. T. Horowitz and V. E. Hubeny, Phys. Rev. D **62**, 024027 (2000) [arXiv:hep-th/9909056].
- [5] V. Cardoso and J. P. S. Lemos, Phys. Rev. D **64**, 084017 (2001) [arXiv:gr-qc/0105103].
- [6] B. Wang, C. Y. Lin and E. Abdalla, Phys. Lett. B **481**, 79 (2000) [arXiv:hep-th/0003295].
- [7] E. Berti and K. D. Kokkotas, Phys. Rev. D **67**, 064020 (2003) [arXiv:gr-qc/0301052].
- [8] R. A. Konoplya, Phys. Rev. D **66**, 044009 (2002) [arXiv:hep-th/0205142]; V. Cardoso, R. Konoplya and J. P. S. Lemos, Phys. Rev. D **68**, 044024 (2003) [arXiv:gr-qc/0305037].
- [9] I. Arsene *et al.* [BRAHMS Collaboration], Nucl. Phys. A **757**, 1 (2005) [arXiv:nucl-ex/0410020]; K. Adcox *et al.* [PHENIX Collaboration], Nucl. Phys. A **757**, 184 (2005) [arXiv:nucl-ex/0410003]; J. Adams *et al.* [STAR Collaboration], Nucl. Phys. A **757**, 102 (2005) [arXiv:nucl-ex/0501009].
- [10] J. J. Friess, S. S. Gubser, G. Michalogiorgakis and S. S. Pufu, JHEP **0704**, 080 (2007) [arXiv:hep-th/0611005].
- [11] S. A. Hartnoll and P. Kovtun, Phys. Rev. D **76**, 066001 (2007) [arXiv:0704.1160 [hep-th]]; S. A. Hartnoll, P. K. Kovtun, M. Muller and S. Sachdev, Phys. Rev. B **76**, 144502 (2007) [arXiv:0706.3215 [cond-mat.str-el]]; S. A. Hartnoll and C. P. Herzog, Phys. Rev. D **76**, 106012 (2007) [arXiv:0706.3228 [hep-th]]; S. S. Gubser, arXiv:0801.2977 [hep-th].
- [12] S. A. Hartnoll, C. P. Herzog and G. T. Horowitz, Phys. Rev. Lett. **101**, 031601 (2008) [arXiv:0803.3295 [hep-th]]; S. A. Hartnoll, C. P. Herzog and G. T. Horowitz, arXiv:0810.1563 [hep-th].
- [13] V. Cardoso, J. Natario and R. Schiappa, J. Math. Phys. **45**, 4698 (2004) [arXiv:hep-th/0403132].
- [14] J. M. Maldacena, Adv. Theor. Math. Phys. **2**, 231 (1998) [Int. J. Theor. Phys. **38**, 1113 (1999)] [arXiv:hep-th/9711200]; E. Witten, Adv. Theor. Math. Phys. **2**, 253 (1998) [arXiv:hep-th/9802150]; S. S. Gubser, I. R. Klebanov and A. M. Polyakov, Phys. Lett. B **428**, 105 (1998) [arXiv:hep-th/9802109].
- [15] S. Hawking and D. Page, Commun. Math. Phys. **87** (1983) 577.

- [16] E. Witten, *Adv. Theor. Math. Phys.* **2**, 505 (1998) [arXiv:hep-th/9803131].
- [17] G. Koutsoumbas, S. Musiri, E. Papantonopoulos and G. Siopsis, *JHEP* **0610**, 006 (2006) [arXiv:hep-th/0606096].
- [18] G. Koutsoumbas, E. Papantonopoulos and G. Siopsis, *JHEP* **0805**, 107 (2008) [arXiv:0801.4921 [hep-th]].
- [19] H. S. Reall, *Phys. Rev. D* **64**, 044005 (2001) [arXiv:hep-th/0104071].
- [20] J. Jing and Q. Pan, *Phys. Lett. B* **660**, 13 (2008) [arXiv:0802.0043 [gr-qc]].
- [21] E. Berti and V. Cardoso, *Phys. Rev. D* **77**, 087501 (2008) [arXiv:0802.1889 [hep-th]].
- [22] X. He, B. Wang, S. Chen, R. G. Cai and C. Y. Lin, arXiv:0802.2449 [hep-th].
- [23] J. Shen, B. Wang, C. Y. Lin, R. G. Cai and R. K. Su, *JHEP* **0707**, 037 (2007) [arXiv:hep-th/0703102]; X. Rao, B. Wang and G. Yang, *Phys. Lett. B* **649**, 472 (2007) [arXiv:0712.0645 [gr-qc]].
- [24] J. P. S. Lemos and V. T. Zanchin, *Phys. Rev. D* **54**, 3840 (1996) [arXiv:hep-th/9511188]; J. P. S. Lemos, *Phys. Lett. B* **353**, 46 (1995) [arXiv:gr-qc/9404041].
- [25] R. B. Mann, *Class. Quant. Grav.* **14**, L109 (1997) [arXiv:gr-qc/9607071]; R. B. Mann, *Nucl. Phys. B* **516**, 357 (1998) [arXiv:hep-th/9705223].
- [26] L. Vanzo, *Phys. Rev. D* **56**, 6475 (1997) [arXiv:gr-qc/9705004].
- [27] D. R. Brill, J. Louko and P. Peldan, *Phys. Rev. D* **56**, 3600 (1997) [arXiv:gr-qc/9705012].
- [28] D. Birmingham, *Class. Quant. Grav.* **16**, 1197 (1999) [arXiv:hep-th/9808032].
- [29] B. Wang, E. Abdalla and R. B. Mann, *Phys. Rev. D* **65**, 084006 (2002) [arXiv:hep-th/0107243].
- [30] R. Aros, C. Martinez, R. Troncoso and J. Zanelli, *Phys. Rev. D* **67**, 044014 (2003) [arXiv:hep-th/0211024].
- [31] D. Birmingham and S. Mokhtari, *Phys. Rev. D* **74**, 084026 (2006) [arXiv:hep-th/0609028].
- [32] A. Sheykhi, arXiv:0709.3619 [hep-th]; M. Nadalini, L. Vanzo and S. Zerbini, arXiv:0710.2474 [hep-th].
- [33] Y. S. Myung, *Phys. Lett. B* **645**, 369 (2007) [arXiv:hep-th/0603200]; arXiv:0801.2434 [hep-th].

- [34] G. Gibbons and S. A. Hartnoll, Phys. Rev. D **66**, 064024 (2002) [arXiv:hep-th/0206202].
- [35] D. Birmingham and S. Mokhtari, Phys. Rev. D **76**, 124039 (2007) [arXiv:0709.2388 [hep-th]].
- [36] R. Emparan, JHEP **9906**, 036 (1999) [arXiv:hep-th/9906040].